Soft Matter

Dynamic Article Links

Cite this: *Soft Matter*, 2011, **7**, 4302

www.rsc.org/softmatter

PAPER

Molecular simulation analysis of structural variations in lipoplexes

Oded Farago[ab] and Niels Grønbech-Jensen[cd]

Received 16th December 2010, Accepted 25th February 2011
DOI: 10.1039/c0sm01498b

We use a coarse-grained molecular model to study the self-assembly process of complexes of cationic and neutral lipids with DNA molecules ("lipoplexes")—a promising nonviral carrier of DNA for gene therapy. We identify the resulting structures through direct visualization of the molecular arrangements and through calculations of the corresponding scattering plots. The latter approach provides a means for comparison with published data from X-ray scattering experiments. Consistent with experimental results, we find that upon increasing the stiffness of the lipid material, the system tends to form lamellar structures. Two characteristic distances can be extracted from the scattering plots of lamellar complexes—the lamellar (interlayer) spacing and the DNA-spacing within each layer. We find remarkable agreement between the computed values of these two quantities and the experimental data [J. O. Rädler, I. Koltover, T. Salditt and C. R. Safinya, *Science*, 1997, **275**, 810–814] over the entire range of mole fractions of charged lipids (CLs) studied experimentally. A visual inspection of the simulated systems reveals that, for very high fractions of CLs, disordered structures consisting of DNA molecules bound to small membrane fragments are spontaneously formed. The diffraction plots of these non-lamellar disordered complexes appear very similar to that of the lamellar structures, which makes the interpretation of the X-ray data ambiguous. The loss of lamellar order may be the origin of the observed increase in the efficiency of lipoplexes as gene delivery vectors at high charge densities.

When DNA molecules are mixed with neutral and cationic lipids (CLs) in an aqueous environment, they spontaneously aggregate to form macromolecular complexes called "lipoplexes". These complexes have attracted much attention over the past two decades because of their potential use as nonviral transfection vectors in gene therapy.[1–5] Transfection is a two-stage process involving adsorption and entry (*via* endocytosis) of the lipoplex into the cell, followed by the release of the DNA to the cytoplasm and delivery to the nucleus, which makes the DNA available for expression.[6–8] CL–DNA complexes exhibit low toxicity and nonimmunogenicity, but their transfection efficiency (TE) remains low compared to that of viral vectors.[6,9] This has spurred intense research activities aimed at enhancing the TE. Recognizing that the structure of CL–DNA complexes may strongly influence their function and TE, much of the effort in theoretical and experimental studies has been devoted to understanding the mechanisms governing complex formation, structure, and phase behavior. X-Ray diffraction experiments have revealed that CL–DNA complexes exist in a variety of mesoscopic structures. These structures include: (i) a multilamellar phase where DNA monolayers are intercalated between lipid bilayers (L_α^C),[10] and (ii) the inverted hexagonal phase with DNA encapsulated within monolayers tubes and arranged on a two-dimensional hexagonal lattice (H_{II}^C).[11]

One of the major advantages of lipoplexes over viral capsids is their ease of preparation and their almost unlimited DNA-carrying capacity, which stem from the fact that the vector is formed by spontaneous self-assembly in aqueous solution. The electrostatic attraction between the anionic DNA and the CLs along with the entropic gain associated with the release of tightly bound counterions from the CLs and DNA are the driving forces for the formation of a complex. In a recent publication, we reported on coarse-grained (CG) simulations of self-assembly of CL–DNA complexes.[12] We demonstrated, in agreement with previous theoretical studies and X-ray scattering experiments,[10,11,13,14] that rigid membranes tend to form lamellar complexes. For soft membranes, the preferred geometry is that of the inverted hexagonal phase. Our simulations also revealed that the phase diagram of the CL–DNA complexes is quite rich and includes, in addition to the lamellar and inverted hexagonal complexes, several other disordered structures with distinct configurational characteristics. We also found a new ordered phase, which has thus far not been observed experimentally,

[a]*Department of Biomedical Engineering, Ben Gurion University of the Negev, Be'er Sheva, 84105, Israel*
[b]*Ilse Katz Institute for Nanoscale Science and Technology, Ben Gurion University of the Negev, Be'er Sheva, 84105, Israel*
[c]*Department of Applied Science, University of California, Davis, California, 95616, USA*
[d]*The Niels Bohr International Academy, The Niels Bohr Institute, Blegdamsvej 17, 2100 Copenhagen, Denmark*

where DNA rods and cylindrical micelles form a 2D square lattice analogous to the 3D cubic NaCl-type structure. Our analysis of the computed self-assembled structures was based on simulation images and on the calculation of the Fourier transform of the DNA positions.[12] The Fourier transform provides a quantitative measure for how the simulated structures would appear in X-ray scattering experiments. To achieve a better comparison with the experimental data, one should also consider the contribution of the lipids to the scattered intensity. By plotting the separate contributions of each component (something which cannot be done experimentally), one can dissect the information displayed in the scattering plots.

In this paper we analyze the scattering intensity plots (the square of the Fourier transform averaged of all angles[12]) of the lamellar complexes, which are formed in our simulations when the DNA is mixed with the stiff lipid material. The technical details of the model and the simulations have been presented in ref. 12. In short, the model is based on the Noguchi–Takasu implicit solvent CG membrane model[15] in which each lipid of length l_{LIP} is represented by a linear rigid molecule[16] consisting of three beads of diameter $\sigma = l_{\mathrm{LIP}}/3 = 6.25$ Å, one of which is hydrophilic and the other two are hydrophobic. The CLs are modeled by associating the hydrophilic bead with a positive unit point charge, while the DNA molecules are modeled as infinitely long parallel rigid rods of diameter $D_{\mathrm{DNA}} = 4\sigma = 25$ Å with uniform charge density corresponding to -1.7 e Å^{-1}. The molecules interact *via* three types of interactions: (i) unscreened electrostatic interactions which are calculated using the Lekner summation method.[17,18] (ii) Short-range repulsive ("hard core") potential. The bead–bead pair potential $U_{\mathrm{rep,bb}}$ is given by Eqn (4) in ref. 15, and the bead–DNA potential $U_{\mathrm{rep,bD}}(r) = U_{\mathrm{rep,bb}}(r - 1.5\sigma)$. Since the DNA rods are strongly repelled from each other by electrostatic forces, there was no need to introduce an additional $U_{\mathrm{rep,DD}}$ term. (iii) The Noguchi–Takasu hydrophobic interaction potential, given by Eqn (5)–(6) in ref. 15. The lipids and the DNA rods are initially randomly distributed within a given volume in the simulation box and, through molecular dynamics (MD) simulations at constant temperature, we follow the evolution of the complexes under different conditions. As the objective of the simulations is to attain self-assembled structures representative of equilibrium, we simulate tens of millions of time steps such that at least half of the total simulated time does not change the characteristics of the visible structures. We have also verified that, while the details of the shown structures do depend on initial conditions, the significant characteristics, such as the peaks in the resulting scattering intensities, are well defined.

We study isoelectric complexes where the total charges on DNA and the CLs neutralize each other, with no added counterions. The structure of the complex is determined as a function of two parameters: (i) the fraction of CLs, ϕ_c, which can be varied by adding different amounts of neutral lipids (NLs), and (ii) the bending modulus, κ_s, which is the prefactor of the bending energy term introduced in the later version of the Noguchi–Takasu model[19] to control the stiffness of the simulated membranes (see Eqn (7) in ref. 12).

Fig. 1 shows the diffraction patterns of stiff complexes ($\kappa_s = 10$) with different values of ϕ_c ranging from $\phi_c = 1$ (a) to $\phi_c = 4/15$ (l). Following the approach outlined in ref. 12, we calculate diffraction patterns from the two-dimensional (2D) Fourier transformation

$$\mathscr{F}(\bar{q}) = \sum_{j=1}^{N} w_j \exp\left(i\bar{r}_j\bar{q}\right), \tag{1}$$

where $\bar{r}_j$ represents the 2D coordinate of the DNA rod or the 2D coordinate of a bead's center of mass in the plane perpendicular to the DNA axis, $\bar{q}$ is the reciprocal lattice vector, and w_j represents the electron density of the jth particle relative to bulk water. For each value of ϕ_c, we show a triplet of figures consisting of (left) the simulated scattered intensity from the DNA rods (with $N = N_{\mathrm{DNA}}$ in eqn (1)), (middle) the simulated scattered intensity from the lipids ($N = 3N_{\mathrm{LIP}}$), and (right) the self-assembled structure of the complex. The displayed scattering intensities are $I(q) \sim \langle|\mathscr{F}(\bar{q})|^2\rangle_\theta$, where $\bar{q} = q\exp(i\theta)$ and $\langle\ldots\rangle_\theta$ denotes the average over all angels. All the DNA scattering plots are drawn on the same scale. The lipid scattering plots are also drawn on the same scale, except for (a)–(e) which are multiplied by the factor indicated on the corresponding plot. The relative scattering intensity of the lipids and the DNA depends on their electron densities, as well as on ϕ_c. Using reasonable values for the electron densities,[20,21] we find that the scale of the DNA intensities is two order of magnitude larger than that of the lipids. Nevertheless, the scattering plots of the lipids exhibit two well identified peaks located at q_{LAM} and $2q_{\mathrm{LAM}}$. These peaks are commonly associated with the lamellar structure. From the position of the first lamellar peak, one can extract the inter-layer lamellar spacing d through $q_{\mathrm{LAM}} = 2\pi/d$. The DNA plots generally exhibit three peaks, two of which coincide with the lamellar peaks from the lipid scattering plots, and one which is commonly referred to as the "DNA peak". The position of the latter at q_{DNA} provides information about the DNA spacing within each layer of the lamellar structure, d_{DNA}. It is assumed that $q_{\mathrm{DNA}} = 2\pi/d_{\mathrm{DNA}}$. Notice that the scattering from the DNA includes the information about the lamellar spacing also observed in the scattering intensity from the lipids. This can be easily understood by considering the idealized lamellar structure sketched in Fig. 2. In this structure, the DNA rods form an oblique lattice with lattice vectors equal to $a_1 = d_{\mathrm{DNA}}$ and $a_2 = d/\sin\theta$. The reciprocal lattice is also oblique with the same angle θ between the lattice vectors $b_1 = 2\pi/d$ and $b_2 = 2\pi/d_{\mathrm{DNA}}$. The peaks which can be seen in the scattering plots of the DNAs correspond to the reciprocal lattice vectors: b_1, $2b_1$, and b_2. These are also the peaks which are usually observed in actual scattering experiments.[10] For idealized lamellar structures, the scattering intensity has peaks at other wavevectors q which correspond to linear combinations of integer-multiples of b_1 and b_2. The positions of these peaks are θ-dependent.[22] In non-idealized complexes, like the ones in our simulations, these peaks are usually very small and are hard to detect in the scattering plots.

Two open arrows are drawn in each of the lipid scattering plots included in Fig. 1. The first one indicates the position of the larger lamellar peak which is located at $q_{\mathrm{LAM}} = 2\pi/d$. The second one denotes the wavevector $2q_{\mathrm{LAM}}$, where we indeed find the second lamellar peak. These two arrows are copied into the corresponding DNA scattering plot, verifying that these peaks are also reproduced by the DNA ordering as explained above. Notice that q_{LAM} is only weakly dependent on ϕ_c. In contrast, the position of the third peak, which is indicated by the solid arrow, varies

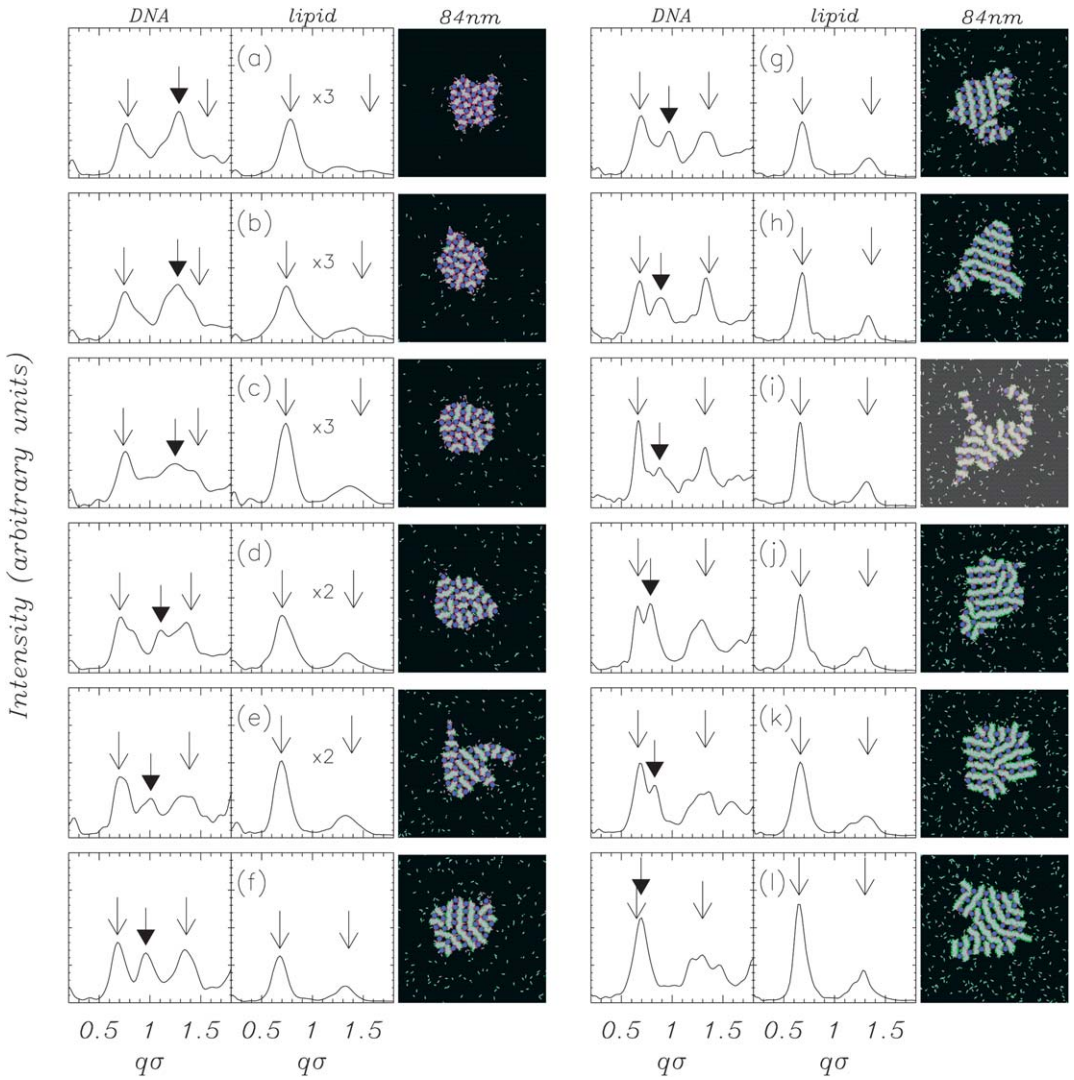

Fig. 1 Self-assembled complex structures consisting of 32 DNA rods mixed with 800 CLs. The amount of NLs varies from 0 ($\phi_c = 1$) in (a) to 2200 ($\phi_c = 4/15$) in (l). Each structure is initiated in a random molecular configuration, and has evolved for 10–50 $\times$ 10^6 MD time steps. The structures are viewed along the DNA axes. Color coding: grey—hydrophobic lipid beads, red—charged hydrophilic heads, green—neutral hydrophilic heads, and blue—DNA rods. For each configuration, the scattering intensities of the DNA rods and the lipids are also plotted. The open arrows indicate the position of the lipid peaks at q_{LAM} and $2q_{\mathrm{LAM}}$. The solid arrow indicate the position of the DNA in-plane correlation peak at q_{DNA}.

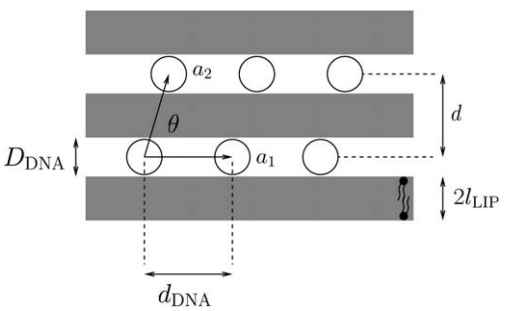

Fig. 2 Sketch of an idealized lamellar complex.

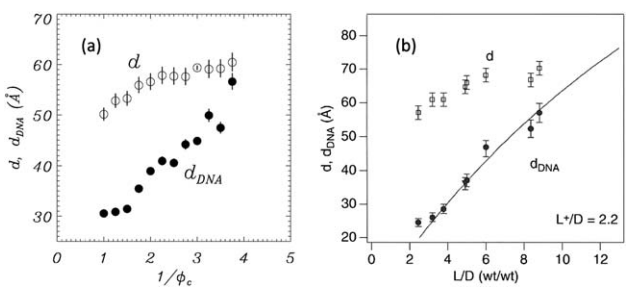

Fig. 3 (a) The inter-layer lamellar spacing d and the DNA-spacing d_{DNA} *vs.* $1/\phi_c$, as computed from the peaks indicated by arrows in the scattering plots shown in Fig. 1. (b) The same quantities derived from synchrotron X-ray scattering data reported in ref. 10. $1/\phi_c = 1$ in (a) corresponds to $L/D = 2.2$ in (b). (b) has been adapted from ref. 10 and 25. Reproduced with permission from Elsevier and AAAS.

noticeably with ϕ_c. This peak is located at $q_{\mathrm{DNA}} = 2\pi/d_{\mathrm{DNA}}$, and the variations in its position reflect the decrease in the DNA spacing with increasing ϕ_c. From the computed scattering plots shown in Fig. 1, we can extract d and d_{DNA} as a function of ϕ_c. Our results are summarized in Fig. 3(a). The visual impression of this

plot is that the results are in overall agreement with the idealized geometry of a lamellar structure shown in Fig. 2. Specifically, the lamellar spacing is well approximated by the sum of twice the length of the lipids and the diameter of the DNA rods, $d \approx (2l_{LIP} + D_{DNA}) \approx 10\sigma = 62.5$ Å. Similarly, the characteristic distance d_{DNA} between DNA rods in each layer approximates a linear relationship with $1/\phi_c$.[10,23,24] This relationship can be derived from the simple geometric consideration that equally spaced DNA rods fill the surface area made available by the lipid bilayer material for any given charge density. There are, however, noticeable deviations from this idealized picture, especially at large ϕ_c. The lamellar spacing decreases below the ideal value, while the DNA spacing attains values higher than predicted by the linear relationship. The origin of these discrepancies becomes clear by inspection of the corresponding structures shown in Fig. 1, where we observe that the long range lamellar order is lost at high ϕ_c in favor of a disordered arrangement of smaller DNA-bilayer fragments. The transition is consistent with previously described membrane rupture at high charge densities resulting from the electrostatic stresses that develop in the complex.[23,24] The highly charged cationic membrane fragments strongly associate with the DNA rods to form the disordered structures seen in Fig. 1(a)–(d). We should not, therefore, be surprised that the values of d and d_{DNA}, which we inferred for lamellar structures, deviate from the expected behavior. The nearly constant behavior of d_{DNA} *vs.* ϕ_c in the disordered phase can be well observed in the structures seen in Fig. 1(a)–(d). The decrease in d in this regime is also consistent with the transition into the disordered phase, where the highly charged cationic membranes become squeezed between the negatively charged DNA rods.

Fig. 3(b) shows the synchrotron X-ray scattering data reported in ref. 10. The agreement with the simulation results in (a) is obvious, lending credibility to our CG model as well as to the Fourier space analysis of the resulting structures. The horizontal axes of the figures express the inverse of the membrane charge density using different scales: $1/\phi_c$in (a) and L/D (the mass ratio between the lipid and DNA material) in (b). The scales are linearly related by: $2.2(1/\phi_c) = L/D$. In both figures, the lamellar spacing approaches the asymptotic value $d \simeq 2l_{LIP} + D_{DNA}$ at small membrane change densities. These asymptotic values are different in the two figures, but this is merely a consequence of the chosen model parameters for l_{LIP} and D_{DNA}, which slightly differ from the experimental values. Both figures exhibit a weak, and very similar, monotonic decrease of d with increasing membrane charge density. For fully charge membranes, the value of d is depressed by about 15–20% compared to the low density asymptote. In ref. 25 this decrease has been attributed to the difference in length between DOPC (neutral) and DOTAP (cationic), the latter being about 6 Å shorter than the former. We, however, observe the same behavior with CLs and neutral lipids, being geometrically identical. Our simulations point to two more explanations for this observation: For moderately charged membranes the effective bilayer thickness slightly shrinks with ϕ_c due to the tensile stress induced by the (negative) electrostatic energy density of a confined charge neutral systems.[17] For high membrane charge density, the decrease in d is likely related to the loss of lamellar order. In this regime, the derived value of $d = 2\pi/q_{LAM}$ does not necessarily coincide with the actual interlayer spacing, since the derivation is based on the presumption that the complex is ideally lamellar.

The agreement between the simulation and experimental results for d_{DNA} is also clear. In both fig. 3(a) and (b), we observe that the DNA spacing drops from $d_{DNA} \approx 60$ Å at low charge densities to $d_{DNA} \approx 30$ Å at high charge densities, in a manner which is well approximated by a linear relationship with the inverse charge density. At very high charge densities, both figures exhibit the same deviation from a linear relationship between d_{DNA} and the inverse charge density. This feature has been attributed in ref. 10 to the limiting contact distance, D_{DNA}, between DNA rods. This interpretation of the results is correct provided that the hydration shell is included in the contact distance. Our results provide yet another possibility. Visual inspection of the self-assembled structures show that the DNA rods do not experience any hard core interactions. The plateau-like behavior of d_{DNA} at high charge densities is related to the formation of disordered structures which enable a more loose packing of the DNA rods.

What we have described in this paper is based on the very close agreement between the computational and experimental results shown in Fig. 3. These results can be explained by a structural shift from lamellar to a fragmented geometry occurring at high membrane charge densities. The fragmentation of the membranes is consistent with the membrane rupture observed in our earlier work described in ref. 23 and 24, where we used a different CG membrane model. This consistency gives us confidence that the loss of structural integrity of the membrane at high charge densities is not an artifact of a particular model. However, we recognize that although this work features the largest complexes ever simulated, there may still be some finite size effects that obscure the comparison with experiments. One such finite size effect is related to the periodic boundary conditions along the DNA axis, which force the infinite DNA rods to lie parallel to each other. This constraint, which simplifies the computational scheme, may lead to the formation of structures with artificial spatial correlations between the DNA rods. Another finite size effect is related to the relatively small sizes of the simulated complexes which, therefore, have scattering plots with peaks that are broader than in the corresponding experimental scattering plots. This low resolution makes it difficult to infer the degree of order from the width of the peaks. Yet another consequence of finite sizes is the enhancement of surface effects. While it seems plausible that the increase in the electrostatic tensile stress at high charge densities does proliferate structural defects, it could be that these defects form more easily on the boundaries of the complex and, therefore, they become over-expressed in our smaller complexes. Nevertheless, the close agreement between Fig. 3(a) and (b), over the entire range of charge densities, supports the possibility that structural variations observed in our simulations may take place in nature. Such a structural shift from lamellar to fragmented geometry should have implications for gene therapy. The shift may explain the improvement in transfection efficiency (TE) exhibited by these complexes at high membrane charge densities.[6] One of the main limiting stages in the transfection process is the release of the genetic material from the complex into the cytoplasm of the host cell. It is indeed reasonable to expect that the DNA rods will be more readily released from the fragmented disordered complexes

than from lamellar structures with long range order. Given the remarkable success of our model, which is based on a highly CG representation of the constituting molecular species and their interactions, it is fair to anticipate the application of this model for obtaining direct observations of the mechanisms governing transfection and gene delivery.

Acknowledgements

We thank Uri Raviv for very useful discussions on X-ray scattering and Cyrus Safinya for his critical reading of the paper. This work was supported by the Israel Science Foundation (Grant Number 946/08). NGJ also acknowledges support from The President's Fund for Visiting Scientists at Ben Gurion University (Israel) and from Danmarks Nationalbank (Denmark).

References

1 P. L. Felgner and G. Rhodes, *Nature*, 1991, **349**, 351–352.
2 Ed. N. Smyth-Templeton and D. D. Lasic, *Gene Therapy. Therapeutic Mechanisms and Strategies*; Marcel Dekker Inc.: New York, 2000.
3 Ed. P. L. Felgner, M. J. Heller, P. Lehn, J.-P. Behr and F. C. Szoka, *Artificial Self-Assembling Systems for Gene Delivery*; American Chemical Society: Washington DC, 1996.
4 A. D. Miller, *Angew. Chem., Int. Ed.*, 1998, **37**, 1768–1785.
5 Ed. L. Huang, M. C. Hung and E. Wagner, *Non-Viral Vectors for Gene Therapy*; Academic Press: San Diego, 1999.
6 K. Ewert, N. L. Slack, A. Ahmad, H. M. Evans, A. J. Lin, C. E. Samuel and C. R. Safinya, *Curr. Med. Chem.*, 2004, **11**, 133–149.
7 S. Huebner, B. J. Battersby, R. Grimm and G. Cevc, *Biophys. J.*, 1999, **76**, 3158–3166.
8 M. T. Kennedy, E. V. Pozharski, V. A. Rakhmanova and R. C. MacDonald, *Biophys. J.*, 2000, **78**, 1620–1633.
9 H. F. Willard, *Science*, 2000, **290**, 1308–1309.
10 J. O. Rädler, I. Koltover, T. Salditt and C. R. Safinya, *Science*, 1997, **275**, 810–814.
11 I. Koltover, T. Salditt, J. O. Rädler and C. R. Safinya, *Science*, 1998, **281**, 78–81.
12 O. Farago and N. Grønbech-Jensen, *J. Am. Chem. Soc.*, 2009, **131**, 2875–2881.
13 D. Harries, S. May, W. M. Gelbart and A. Ben-Shaul, *Biophys. J.*, 1998, **75**, 159–173.
14 S. May, D. Harries and A. Ben-Shaul, *Biophys. J.*, 2000, **78**, 1681–1697.
15 H. Noguchi and M. Takasu, *Phys. Rev. E: Stat. Phys., Plasmas, Fluids, Relat. Interdiscip. Top.*, 2001, **64**, 041913.
16 H. Tapia-McClung and N. Grønbech-Jensen, *J. Polym. Sci., Part B: Polym. Phys.*, 2005, **43**, 911–916; H. Tapia-McClung and N. Grønbech-Jensen, *J. Polym. Sci., Part B: Polym. Phys.*, 2010, **48**, 2604–2605.
17 N. Grønbech-Jensen, *Int. J. Mod. Phys. C*, 1997, **8**, 1287–1297.
18 N. Grønbech-Jensen, *Comput. Phys. Commun.*, 1999, **119**, 115–121.
19 H. Noguchi, *Phys. Rev. E: Stat. Phys., Plasmas, Fluids, Relat. Interdiscip. Top.*, 2003, **67**, 041901.
20 U. Raviv, D. J. Needleman, Y. Li, H. P. Miller, L. Wilson and C. R. Safinya, *Proc. Natl. Acad. Sci. U. S. A.*, 2005, **102**, 11167–11172.
21 U. Raviv, Private Communication, 2010.
22 T. Ben-Nun, A. Ginsburg, P. Székely and U. Raviv, *J. Appl. Crystallogr.*, 2010, **43**, 1522–1531.
23 O. Farago, N. Grønbech-Jensen and P. Pincus, *Phys. Rev. Lett.*, 2006, **96**, 018102.
24 O. Farago and N. Grønbech-Jensen, *Biophys. J.*, 2007, **92**, 3228–3240.
25 C. R. Safinya, *Curr. Opin. Struct. Biol.*, 2001, **11**, 440–448.

